Chains of Trans-Edge-Sharing Molybdenum Octahedra: Metal–Metal Bonding in Extended Systems

Timothy Hughbanks and Roald Hoffmann*

Contribution from the Department of Chemistry and Materials Science Center, Cornell University, Ithaca, New York 14853. Received November 5, 1982

Abstract: A detailed analysis of bonding in systems with chains of condensed molybdenum octahedra is given. A one-dimensional model proves to be applicable over the range of molybdates yet synthesized. The electronic coupling between chains is discussed. Distortions in newly synthesized quaternary systems are seen to result from increased electron count on the molybdenum chains. The band theoretic explanation of these distortions parallels the treatment of second-order Jahn–Teller distortions.

The old and new chemistry of metal-rich halides, chalcogenides, and oxides provides us with a magnificent array of metal–metal bonded clusters, chains, and networks.[1] M_6 octahedra are fundamental building blocks in these condensed systems. Among the simpler chalcogenide systems are compounds such as Ti_5Te_4,[2] Nb_5Se_4, and Nb_5Te_4[3] which contain vertex-sharing octahedra of metals and $Tl_2Mo_6Se_6$[4] or $Tl_2Fe_6Te_6$[5] which exhibit chains of face-sharing metal octahedra. Halide systems seem to demonstrate proclivity toward edge-sharing octahedra in forming chains.[6] The sesquihalides Gd_2Cl_3,[7] Y_2Cl_3,[8] Tb_2Cl_3, Er_2Cl_3, and Lu_2Cl_3[9] and bromide analogues are all isotypic and contain trans-edge-sharing chains of rare earth metals. Sc_5Cl_8 exhibits chains with the same metal framework but differing anion environment.[10] The Sc_5Cl_8 structure is shown in Figure 1. This compound is characterized as containing conventional Sc(III) ions residing in the octahedral sites of the ordinary chains of this structure and low valent Sc within the edge-sharing Sc–Sc bonded framework. The "average" Sc of this chain is $d^{1.75}$; i.e., there are 7 e/Sc_4 unit available for Sc–Sc bonding.

Further condensation of single chains to form various double chains has been observed in Er_7I_{10},[11] Sc_7Cl_{10},[12] Tb_6Br_7, and Er_6I_7[13] as well as to form double layers as in $ScCl$,[14] YCl,[8] $LaBr$, and many other rare earth halides.[15] A number of double layer compounds as well as Gd_2Cl_3, Nb_3I_8,[16] and NbI_4[17] have been

theoretically investigated by Bullett.[18] The LCAO treatment put forth in his important paper largely accounts for the observed properties of the systems investigated.

In the present work we confine out attention to oxide systems. In particular, we consider systems containing chains of trans-edge-sharing octahedra. The structural chemistry of these systems, initiated with the synthesis of $NaMo_4O_6$ by Torardi and McCarley,[19,20] continues to be developed in the laboratory of McCarley and co-workers. While there are obvious similarities between the Mo–oxide chains (described below) and the chains found in Sc_5Cl_8, there are some very important differences: (a) The chains are much more electron rich than any halide systems yet synthesized. While the halide chains contain no more than 7 e/M_4 unit, the molybdates have formal d occupancies of at least 13 e/Mo_4. (b) The oxide anions are much smaller than halides (or chalcogenides). This effectively allows much more flexibility for Mo–Mo bonding. (c) Metal–metal distances within the chains are much shorter than in group 3 or rare-earth halides—a result of factors a and b. What follows is a more detailed picture of bonding in these molybdenum oxide compounds.

The $NaMo_4O_6$ System

The structure of $NaMo_4O_6$, shown in Figure 2, consists of two "Mo_4O_4" chains per unit cell which are linked by trigonally bonded oxygen atoms. Na^+ ions occupy eight-coordinate sites in the channels between the cross-linked chains. The crystal system appropriate for this structure is simple tetragonal (space group $P4/mbm$). The Mo–Mo bond lengths are as displayed in **1**.

1
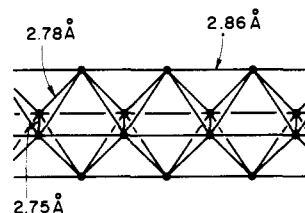
We performed band structure calculations on a $Mo_8O_{12}^{2-}$ extended system (the $NaMo_4O_6$ structure sans Na^+ ions) along several symmetry lines in the first Brillouin zone for this tetragonal system.[21] Figure 3 displays the energy bands plotted along the lines indicated. The energy range shown includes only the Mo d bands, the O s and p bands lying lower. In these and subsequent calculations we idealized the structure so that all Mo–Mo bonds were 2.8 Å, Mo–O bonds within the "Mo_4O_4 chains" were taken

(1) For a review see: Simon, A. *Angew. Chem.* **1981**, *93*, 23–44; *Angew. Chem., Int. Ed. Engl.* **1981**, *20*, 1–22. See also: von Schnering, H. G. *Angew. Chem.* **1981**, *93*, 44–63; *Angew. Chem., Int. Ed. Engl.* **1981**, *20*, 33–51.
(2) Grønvold, F.; Kjekshus, A.; Raaum, F. *Acta Crystallogr.* **1961**, *14*, 930–934.
(3) Selte, K.; Kjekshus, A. *Acta Chem. Scand.* **1963**, *9*, 2560–2562.
(4) Potel, M.; Chevrel, R.; Sergent, M. *Acta Crystallogr., Sect. B* **1980**, *B36*, 1545–1548; *J. Solid State Chem.* **1980**, *35*, 286–290.
(5) Klepp, K.; Boller, M. *Monatsh. Chem.* **1979**, *110*, 677–684.
(6) Corbett, J. D. *Acc. Chem. Res.* **1981**, *14*, 239–246; "Solid State Chemistry: A Contemporary Overview"; Holt, S. L., Milstein, J. B., Robbins, M., Eds.; American Chemical Society: Washington, D. C., 1980; Chapter 18.
(7) Lokken, D. A.; Corbett, J. D. *Inorg. Chem.* **1973**, *12*, 556–559.
(8) Mattausch, Hj.; Hendricks, J. B.; Eger, R.; Corbett, J. D.; Simon, A. *Inorg. Chem.* **1980**, *19*, 2128–2132.
(9) Simon, A.; Holzer, N.; Mattausch, Hj. *Z. Anorg. Allg. Chem.* **1979**, *456*, 207–216.
(10) Poeppelmeier, K. R.; Corbett, J. D. *J. Am. Chem. Soc.* **1978**, *100*, 5039–5044.
(11) Berroth, K.; Simon, A. *J. Less-Common Met.* **1980**, *76*, 41–54.
(12) Poeppelmeier, K. R.; Corbett, J. D. *Inorg. Chem.* **1977**, *16*, 1107–1111.
(13) Berroth, K.; Mattausch, Hj.; Simon, A. *Z. Naturforsch., B: Anorg. Chem., Org. Chem.* **1980**, *B35*, 626–630.
(14) Poeppelmeier, K. R.; Corbett, J. D. *Inorg. Chem.* **1977**, *16*, 294–297.
(15) (a) Simon, A.; Mattausch, Hj.; Holzer, N. *Angew. Chem.* **1976**, *88*, 685–686; *Angew. Chem., Int. Ed. Engl.* **1976**, *15*, 624–625. (b) Mattausch, Hj.; Simon, A.; Holzer, N.; Eger, R. *Z. Anorg. Allg. Chem.* **1980**, *466*, 7–22.
(16) Simon, A.; von Schnering, H. G. *J. Less-Common Met.* **1966**, *11*, 31–46.
(17) (a) Corbett, J. D.; Seabaugh, P. *J. Inorg. Nucl. Chem.* **1958**, *6*, 207–209. (b) Dahl, L. F.; Wampler, D. L. *J. Am. Chem. Soc.* **1959**, *81*, 3150–3151. (c) Dahl, L. F.; Wampler, D. L. *Acta Crystallogr.* **1962**, *15*, 903–911.

(18) Bullett, D. W. *Inorg. Chem.* **1980**, *19*, 1780–1785.
(19) Torardi, C. C.; McCarley, R. E. *J. Am. Chem. Soc.* **1979**, *101*, 1963–1964.
(20) A similar compound with stoichiometry $Ba_5(Mo_4O_6)_8$ was also reported: Torardi, C. C.; McCarley, R. E. *J. Solid State Chem.* **1981**, *37*, 393–397.
(21) Lax, M. "Symmetry Principles in Solid State and Molecular Physics"; Wiley: New York, 1974.
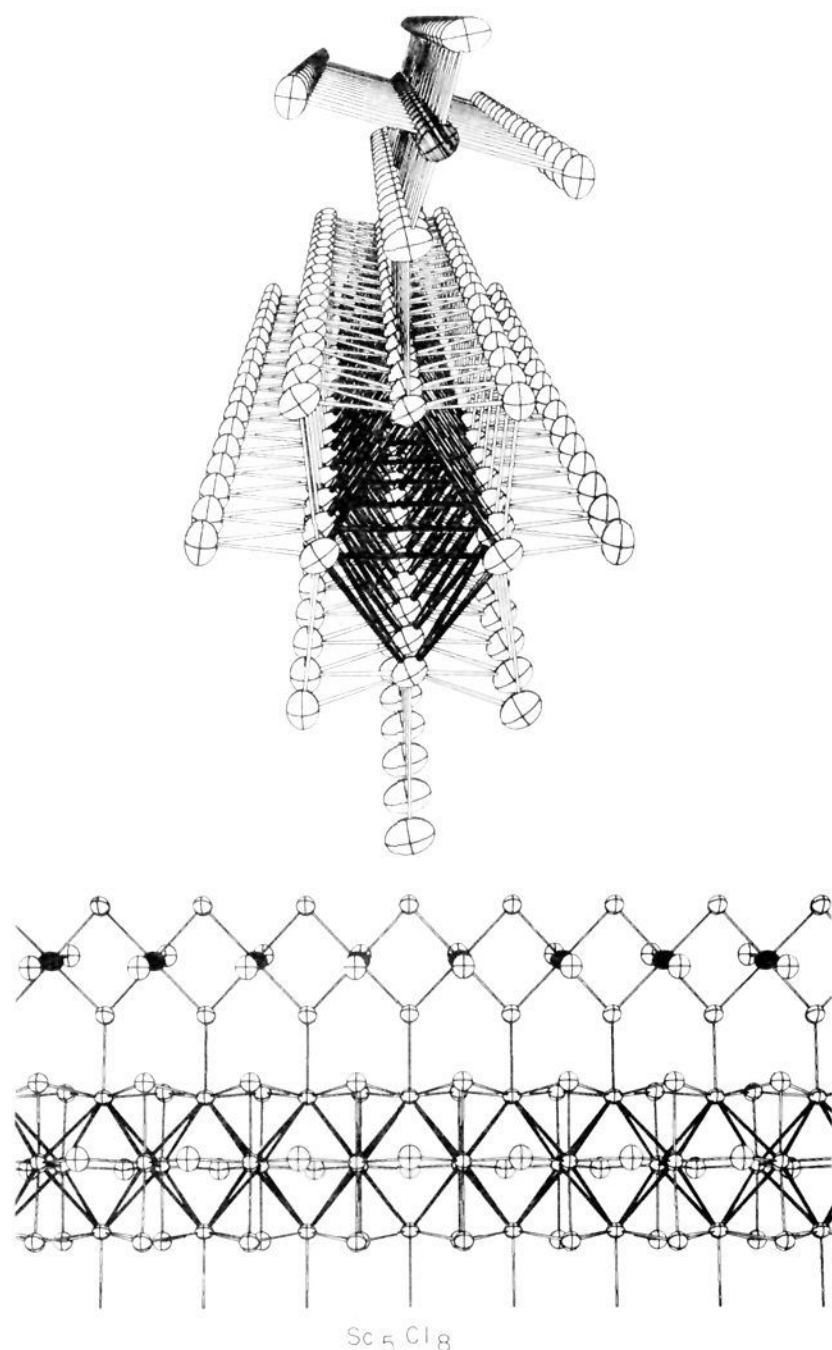
Figure 1. The Sc_5Cl_8 structure is viewed down the chain axes and from the side. The Sc–Sc linkages are darkened, as are the Sc(III).

Table I. Atomic Orbital Occupations for Molybdenum

	orbital	filled O bands (<13 eV)	filled Mo bands (>13 eV, $<\epsilon_F$)
apical Mo	"t_{2g}" $\begin{cases} x^2 - y^2 \\ xz \\ yz \\ z^2 \end{cases}$	0.18 / 0.12 / 0.12 / 0.32	0.64 / 0.66 / 0.97 / 0.28
	xy	0.31	~0
basal Mo	"t_{2g}" $\begin{cases} x^2 - y^2 \\ xz \\ yz \\ z^2 \end{cases}$	0.08 / 0.16 / 0.16 / 0.27	0.82 / 0.74 / 0.65 / 0.13
	xy	0.24	0.39

at 2.07 Å, and distances between Mo and trigonal O were 2.01 Å.

We will not attempt to understand Mo–Mo bonding in this system using the band structure for the full three-dimensional $Mo_8O_{12}{}^{2-}$ system but shall instead consider a one-dimensional model system consisting of a single edge-sharing chain. First, however, we will take a closer look at the general features of Figure 3. The most important feature in this figure is the anisotropy in the energy band dispersion curves. On the lines Z → A and M → Γ the bands are generally quite flat, while the Γ → Z and A → M lines display curves with much larger slopes. The interpretation of this state of affairs is straightforward. As we move along the horizontal lines of the Brillouin zone (Z → A, Γ → M, etc.), we are investigating the variations in crystal orbital energies as we vary the orbital phases on different chains. In other words, if there were no electronic communication whatsoever between


$Na^+ (Mo_4O_6^-)$

● Mo   ○○ O
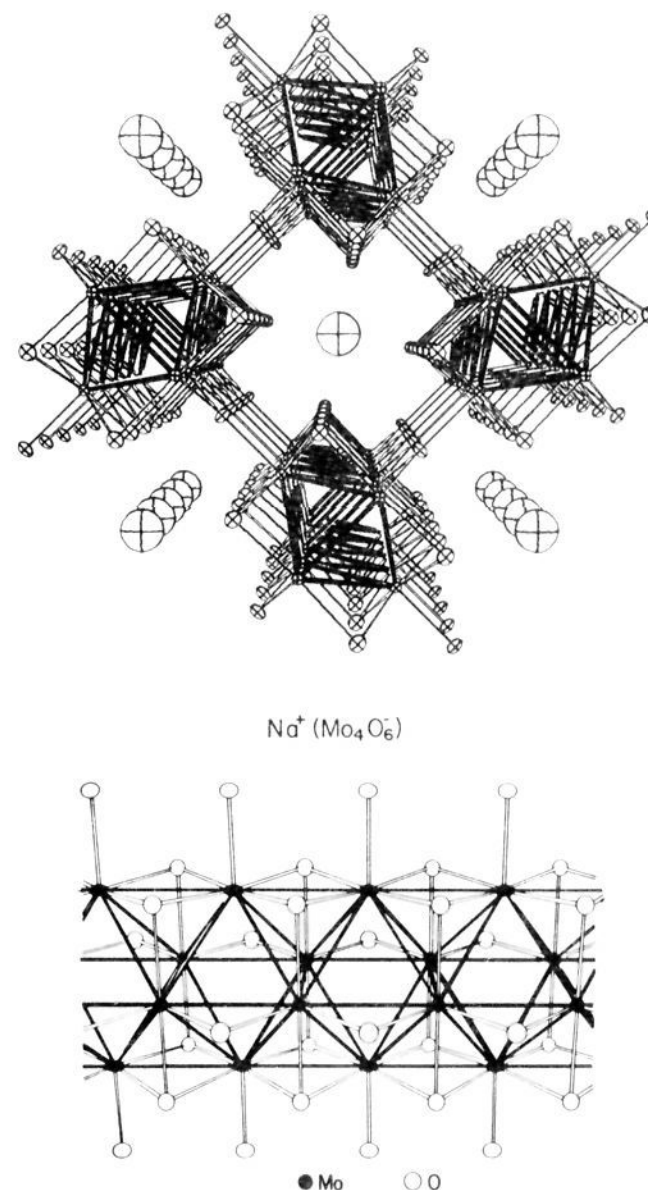
Figure 2. The $NaMo_4O_6$ structure, viewed down the chain axes and from the side of an isolated chain. The trans-edge-sharing Mo–Mo chains are darkened.
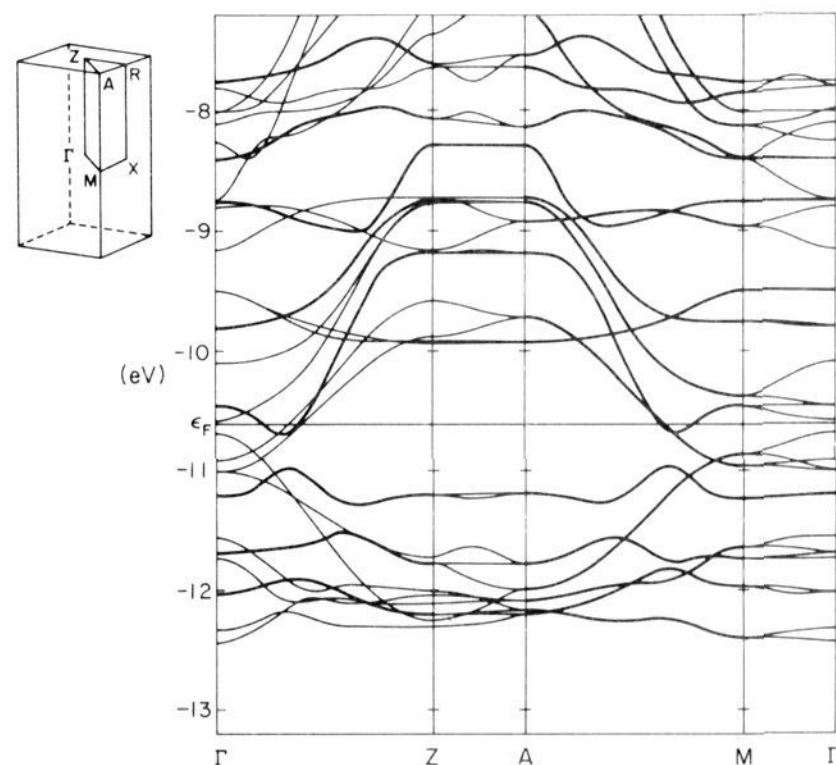
Figure 3. The Mo d bands are displayed along selected symmetry lines for a $Mo_8O_{12}{}^{2-}$ system. The Γ → Z and M → A lines are parallel to the chain axes. Heavier lines indicate doubly degenerate dispersion curves.

the Mo d orbitals of the different chains in the crystal, the curves on the Z → A and M → Γ lines would be totally flat; the extent to which Z → A and M → Γ lines are indeed flat reflects the weak interchain coupling provided by the linking trigonal oxygens. While we will return to the question of interchain coupling below, at present we turn our attention to a one-dimensional model for understanding bonding within the chains.

We have chosen to model the chains in $NaMo_4O_6$ in the following way: to the Mo_4O_4 "core" we add O–H groups to "tie off"
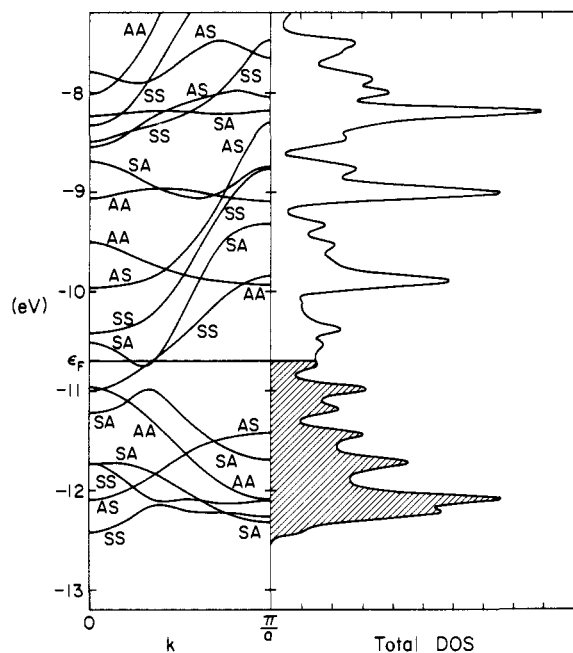
Figure 4. The d band structure and DOS are shown for the one-dimensional model system. Shaded levels in the DOS are those occupied for a 13-electron system. The band labels pertain to the mirror planes of Figure 5.

the basal Mo atoms and pseudohydrogen atoms ("H"), to complete the coordination of the apical metal atoms, as illustrated in **2**. The
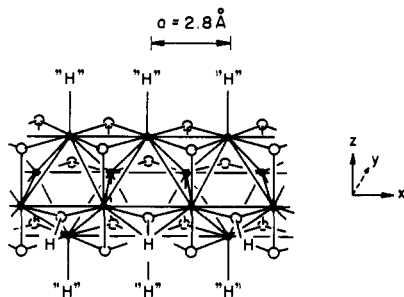

2

pseudohydrogens are defined with $H_{ss} = -15.0$ eV, $\zeta = 2.2$, and a Mo–"H" distance of 1.7 Å, enabling us to mimic the σ-bonding characteristics of an oxygen atom. The electron count on the chain was chosen to preserve the formal oxidation state of Mo in $NaMo_4O_6$ (13 e/Mo_4).

In Figure 4, we show the one-dimensional band structure calculated for our model chain. At right in the figure is the density of states (DOS) with shaded levels being those which are occupied. The close similarity between the model one-dimensional band structure in Figure 4 and the curves seen in Figure 3 on the $\Gamma \rightarrow Z$ and $M \rightarrow A$ lines is indicative of the appropriateness of our one-dimensional model in examining Mo–Mo bonding. Each of the bands in Figure 4 carries two labels by which they are classified according to the symmetry exhibited by the corresponding crystal orbitals with respect to reflections in the vertical (xz) and horizontal (xy) mirror planes. Figure 5 shows the relationship between these mirror planes and the Mo framework for the chain. The first label pertains to the reflection symmetry with respect to the vertical plane, and the second pertains to the horizontal plane—where S and A stand for symmetric and antisymmetric.

Unfortunately, even our one-dimensional model displays a complexity which makes a detailed understanding of the energy bands tedious (though not especially difficult) and beyond that needed for a general understanding of the electronic structure. We will rely on simpler, if less precise, methods of analysis. In later discussion we will, however, return to consider selected crystal orbitals as necessary.
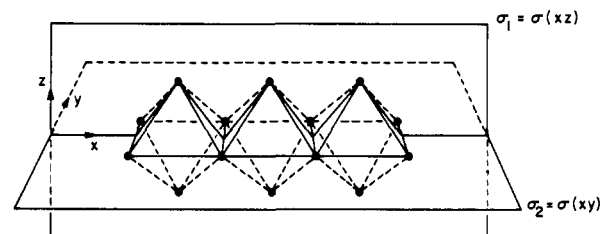
Figure 5. Mirror planes used in classifying the bands of Figure 4. σ_1 pertains to the first labels and σ_2 to the second labels.

Embedded within the chains of these molybdates are two common inorganic "molecular fragments", ML_5 and ML_4 (see **3**, only M–O bonds drawn). We are identifying the local Mo–O
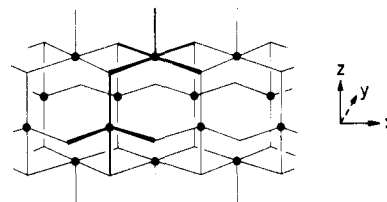
3

coordination environments with those of common inorganic fragments. With this fragmentation mode, we can build a general scheme for interpreting the rather complex electronic structure of these compounds. Of course, such a scheme will necessarily be rough since the "L atoms" are, in this case, shared among as many as three fragments. More to the point, however, is the fact that this scheme will simplify consideration of Mo–Mo bonding by first "eliminating" Mo orbitals which are primarily used in Mo–O bonding (or, in crystal field language, we factor out those Mo orbitals which are pushed up by the oxide crystal field).

Adopting the coordinate system used in **2** and **3**, the appropriate frontier molecular orbitals for our ML_4 and ML_5 fragments are as in **4a** and **4b**, respectively. Both of these fragments may be
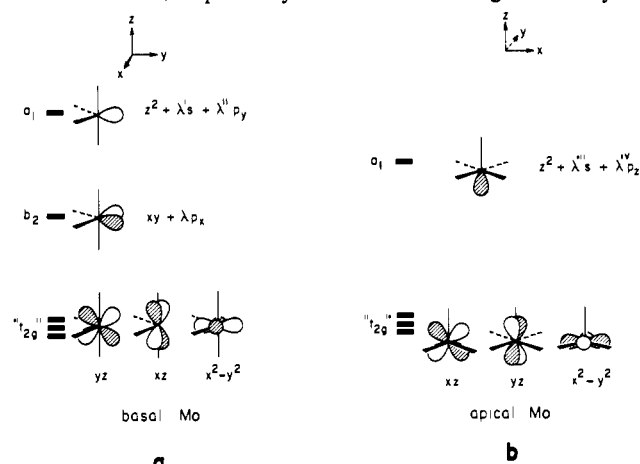
4

seen as remnants of an octahedron from which one or two ligands have been removed. The three low-lying orbitals for both fragments are the descendants of the octahedral t_{2g} sets. The higher lying orbitals (one in ML_5, two in ML_4) are hybrids which are left behind as we remove ligands. A more thorough discussion may be found elsewhere.[22] Indicated in **4** is the atomic orbital composition of various fragment orbitals; the numbers λ, λ', etc. are coefficients which specify the degree of hybridization and are considerably less than unity.

Using the fragments' orbitals in **4**, we now construct an elementary scheme for the Mo bands of the chain. Because the
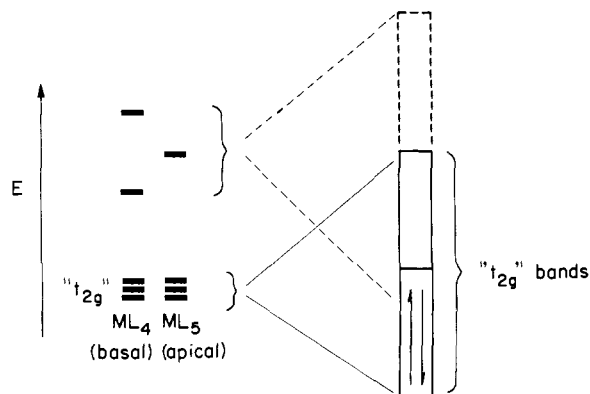
(22) Elian, M.; Hoffmann, R. *Inorg. Chem.* **1975**, *14*, 1058–1076.

Figure 6. A schematic picture of the chain Mo band structure.

fragment "t_{2g}" blocks are at low energy, we expect the largest contribution to Mo–Mo bonding should arise from these orbitals. The extent to which the upper fragment orbitals make a contribution will depend upon the relative strength of the Mo–Mo vs. Mo–O interactions; if the splittings between the "t_{2g}" blocks and the upper hybrids is larger than the width of the Mo bands formed upon interacting the "fragments", then the contribution of the upper orbitals should be small. The formal average d count of 3.25 should be borne in mind since this implies that only the bottom half of the "t_{2g}" bands will be filled even without any participation of the upper hybrid orbitals. Figure 6 schematically displays these qualitative features.

The essential validity of the above description may be confirmed by examination of the Mulliken population analysis of the crystal orbitals resulting from our one-dimensional model. In Table I we show the occupations of the Mo d orbitals in the Mo d band region and below (i.e., in the O s and p bands). As the table indicates, d orbital contributions within the Mo bands are made primarily by the "t_{2g}" orbitals. Conversely, the remaining d orbitals make relatively larger contributions in the O bands as we would expect on the basis of their use in Mo–O σ bonding.

To gain more information about the Mo–Mo bonding, we will inspect overlap population data extracted from our model system. The overlap population[23] between two atoms, useful as a measure of bond strength, depends upon the total number of occupied molecular orbitals. Alternatively, one may wish to single out the contribution to the total overlap population between two atoms made by *each* molecular orbital. Proceeding along these lines, we present below curves which show graphically the contribution of the individual *crystal* orbitals to the overlap populations between particular atom pairs as a function of the orbital energies. The interpretation of these curves is straightforward: over energy ranges where the curves are positive the crystal orbitals make a bonding contribution between the two atoms in question; where they are negative an antibonding contribution is made. An alternative view is to say that we are constructing a "weighted" density of states (DOS) curve: for the levels in a given energy range the total DOS in that range is weighted by the contribution to the overlap population made by the orbitals in that range. The resulting curves enable one to ascertain the bonding characteristics of levels in a given energy range with respect to any pair of atoms. Let us call the quantity plotted "crystal orbital overlap population" or COOP. It should be clear that COOP is an extension of the Mulliken population analysis formalism to the infinite crystalline case.

In Figure 7 we show COOP curves for the four unique Mo–Mo bonds of $NaMo_4O_6$ obtained from our one-dimensional model calculations. The normalization of these curves is arbitrary but the relative magnitudes are consistent between the curves. The total overlap populations at the Fermi level (formal d count of 3.25) are given in Table II. These are obtained by integrating our COOP curves up to the Fermi level. The contributions to Mo–Mo overlap populations made by lower lying levels (the "O
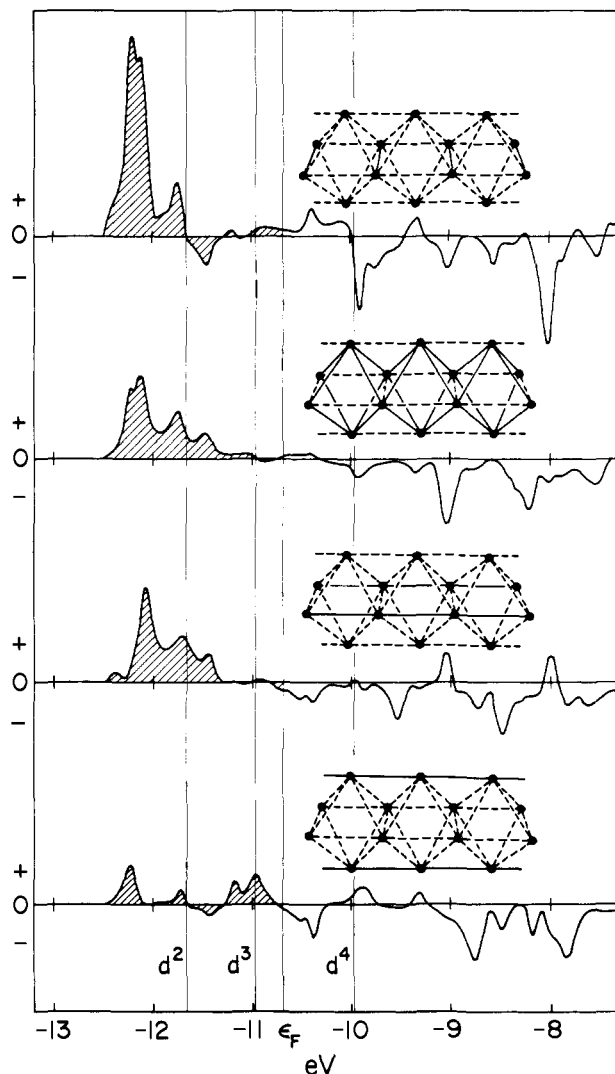
(23) Mulliken, R. S. *J. Chem. Phys.* **1955**, *23*, 1833–1846, 2343–2346.

Figure 7. Crystal orbital overlap population curves for the Mo–Mo bonds of the edge-sharing chains. Unbroken lines in the accompanying insets indicate which bonds correspond to each curve.

Table II. Total Overlap Populations for Mo–Mo Bonds

	for occupation up to ϵ_F	for "optimal" occupation
Mo (basal)–Mo (basal), in cell	0.31	0.36
Mo (basal)–Mo (basal), intercell	0.21	0.22
Mo (basal)–Mo (apical)	0.22	0.23
Mo (apical)–Mo (apical)	0.10	0.10

bands") are all less than 0.02, and therefore the values in Table II are nearly what would be obtained by integrating the curves in Figure 7 up to the Fermi level, disregarding deeper levels. The "optimal" occupations in Table II are the maximum possible values achievable by varying the number of electrons continuously—these values correspond to different occupations for each bond and could not actually be attained simultaneously but are merely upper bounds.

Figure 7 shows some striking features. We see that there is an evident general segregation between Mo–Mo bonding and antibonding levels. Furthermore, as underscored in Table II, the electron occupancy in this system is nearly optimal in that bonding and antibonding levels are respectively occupied and vacant. Also conspicuous is the marked differences in "bond strengths" indicated by the overlap populations. The pairs of basal Mo atoms shared by adjacent metal octahedra appear rather strongly bonded while apical Mo atoms of neighboring octahedra show a much smaller

3532 *J. Am. Chem. Soc., Vol. 105, No. 11, 1983*

Hughbanks and Hoffmann

overlap population. The reasons for these important differences will be discussed below. The extent to which these overlap population asymmetries are reflected in the chain structure can be seen in **1**. While the bond length trend seen in the structure is as predicted on the basis of Figure 7 and Table II, the magnitude of the variations may seem disappointing. However, the bond length variations are obviously not independent; e.g., distances between apical atoms must be the same as between basal atoms of neighboring octahedra. Only a distortion which changes the crystal symmetry can alter these fixed relationships.

We now turn to questions of electron counting and consider structural variations expected as a function of the formal molybdenum d count. With Figure 7 as a guide, we come to the following conclusions: (1) As the number of electrons increases up to a d^4 count, bonds *parallel* to the chain axis should lengthen somewhat while distances between the shared basal atoms might be expected to shorten slightly as the corresponding overlap population becomes optimal. (2) For any systems with more than 4 e/metal, all Mo–Mo distances should begin to increase as antibonding levels are occupied—this is particularly evident for the shared basal atoms. (3) Electron counts below d^2 should also lead to longer metal–metal distances, but the shared bonds between basal atoms should remain shorter in all cases. Support for this contention is found in Sc_5Cl_8[10] where chains in which the metals are formally $d^{1.75}$ exhibit precisely the structural features expected. Close Cl$\cdots$Cl contacts undoubtedly prevent Sc–Sc distances for "bonds" parallel to the chain axis from being too much shorter than the observed 3.52 Å, however.

Having examined the consequences of our calculated overlap populations we are left with the question of *why* we should expect Mo–Mo bond "strengths" to be different from bond to bond. One clue stems from a structural observation: The calculated overlap populations decrease as the number of oxygen atoms which bridge the bond in question increases. Bonds joining apical Mo atoms are bridged by two oxygens, and the shared basal Mo–Mo bonds are unbridged. The effect of bridging donor atoms on metal–metal bonding has been examined in detail for bridged M_2L_{10} complexes in earlier work.[24] Metal d levels in these dimers were described in two regimes: (a) for compounds with short M–M distances the conventional $\sigma < \pi < \delta \sim \delta^* < \pi^* < \sigma^*$ ordering is obeyed, (b) for compounds with long M–M distances the ordering imposed by direct through-space interaction is entirely transcended by through-bond M–L–M interactions. In the present compounds, with Mo–Mo $\simeq$ 2.8 Å, we are in an intermediate situation; although metal–metal bonding is important, the bridging oxides serve to significantly dilute it. Thus, of all the curves shown in Figure 7, that for bonds between octahedral apices are least differentiated into bonding and antibonding regions.

A contributing factor to the relative strength of bonds between shared basal atoms is the fact that such bonds are not subject to "trans effect", that is, these bonds are not counterbalanced by oppositely directed M–M bonds. To see how such an effect is manifested in the crystalline case, we will select some occupied crystal orbitals for direct examination. Shown in a "top view" in **5**, is an orbital contributing significantly to σ bonding between apical as well as basal metals. Because this orbital is unaltered upon primitive translation along the chain axis, it corresponds to an orbital for which $k = 0$ (this orbital is in fact the lowest energy metal-based orbital at $k = 0$). By contrast, the orbital displayed in **6** exhibits σ-bonding character only between the shared basal atoms. This orbital changes sign upon translation and therefore has wavevector π/a.

Although we have used a specific crystal orbital to demonstrate it, the fact that orbitals at the zone edge cannot contribute to Mo–Mo σ bonding for bonds parallel to the chain axis is general. It is a simple consequence of the inversion symmetric property of d orbitals and the fact that orbitals at the zone edge are out of phase from cell to cell. An exactly analogous line of reasoning leads one to the conclusion that π bonding (using d orbitals) will
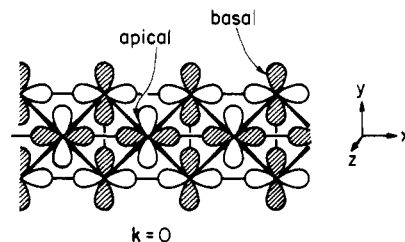

5
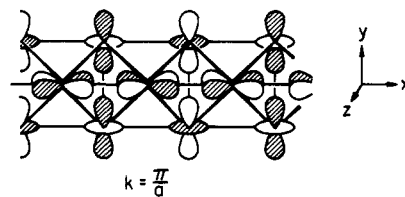
6

be realized for bonds parallel to the chain axis only in crystal orbitals at the zone edge (e.g., see **6** above). In either case the conclusion is the same: because crystal orbitals may make bonding contributions to bonds parallel to the chain axis in a restricted region of k space, the total bonding will be less than for bonds perpendicular to the chain axis where bonding contributions occur at all k. Such is the band theoretic language which underpins what is most simply described as a trans effect[25] in ordinary chemical language.

Interchain Coupling

In the preceding we analyzed the metal–metal bonding in $NaMo_4O_6$ by using a one-dimensional model system. This was possible because the bridging three-coordinate oxygens only weakly coupled crystal orbitals on neighboring chains. The weakness of this perturbation is manifested in Figure 3 in band curves on the $Z \rightarrow A$ and $M \rightarrow \Gamma$ lines were dispersions of ≤ 0.3 eV are seen. Our one-dimensional model thus provides a band structure very similar to what is seen on the more interesting $\Gamma \rightarrow Z$ and $M \rightarrow A$ lines. However, it is not obvious that the interchain coupling should appear so weak.

As we have seen, the major contributions to the band structure are made by the quasi-t_{2g} orbitals of the metals. Consequently, the principal mechanism for coupling the chains would be via Mo d–O p π interaction as, for example, in **7**. We would then expect crystal orbitals with large contributions from apical yz or basal xz or yz orbitals to be most strongly coupled by this type of interaction.
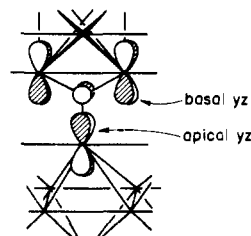

7

To estimate the magnitude of splitting induced by the d–p π interaction, we might consider a simple two-dimensional example such as is provided by a MoO_2 net as shown in **8**. The structure **8** is a two-dimensional analogue of the well-known perovskite structure (e.g., ReO_3) in which MO_6 octahedra share oxide

(24) Shaik, S.; Hoffmann, R.; Fisel, C. R.; Summerville, R. H. *J. Am. Chem. Soc.* **1980**, *102*, 4555–4572.

(25) Although the context is different, our discussion is not really so distinct from usual trans effect arguments. See, for example: Burdett, J. K.; Albright, T. A. *Inorg. Chem.* **1979**, *18*, 2112–2120.
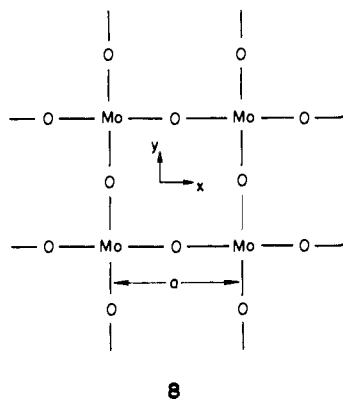
8

corners. Of particular interest in this context is the energy difference between the two crystal orbitals in **9a** and **9b**. This energy

a   **b**
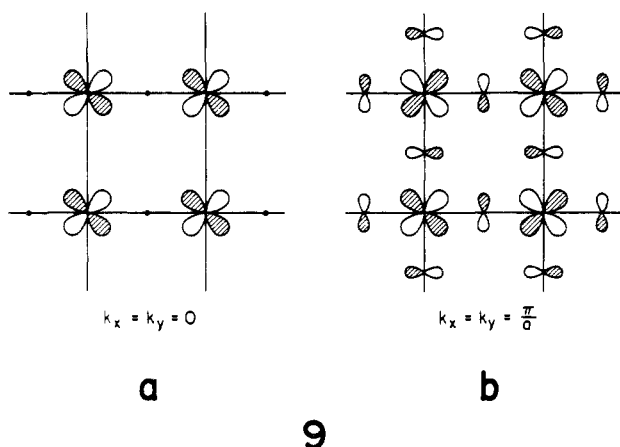
9

difference will provide a good estimate of the splitting of the "t_{2g}" d orbitals in ReO$_3$. (**9a** is essentially "nonbonding" and **9b** represents the extreme in Mo–O d–p π antibonding.) For MoO$_2$ with Mo–O = 2.07 Å, we calculate this energy difference to be 1.1 eV. This value is not small when compared with bandwidths we have seen for our one-dimensional model chain. Thus, the question is posed, why is the d–p π interaction giving much smaller dispersions in NaMo$_4$O$_6$?
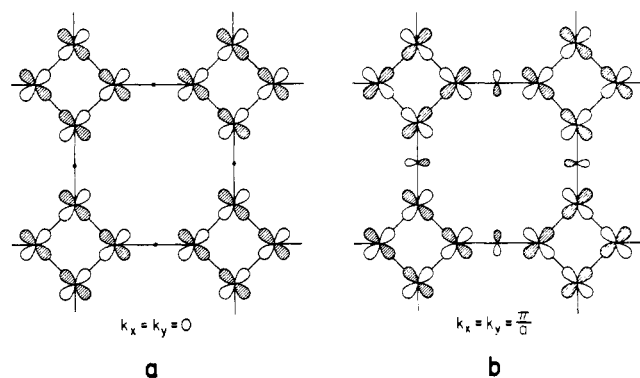
We will address the above question by considering a second example: a hypothetical Mo$_4$O$_2$ net as in **10**. **10** is obtained from
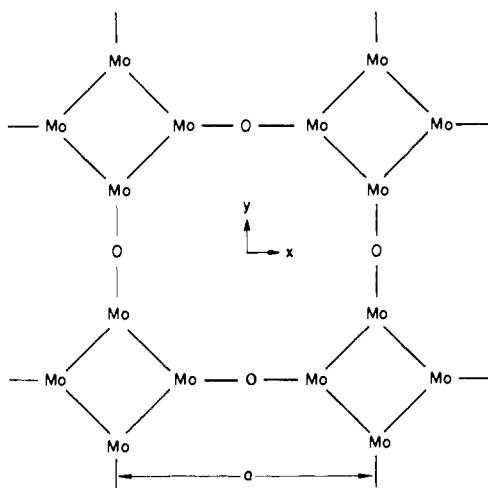
10

8 by replacing each Mo atom by a Mo$_4$ square. We took Mo–Mo = 2.8 Å, although this choice is of no consequence for the point

we wish to make here. We now consider the energy difference between the crystal orbitals shown in **11a** and **11b**. Although

a   **b**

11

the physical origin of the splitting of the **11a** and **11b** crystal orbitals is the same as in the case of **9a** and **9b**, the magnitude of the splitting is much smaller: 0.3 eV. The most important reason for this smaller splitting is the fact that Mo$_4$ fragment orbital is delocalized over *four* metal atoms.

To be more explicit, delocalization is responsible for a reduction in the d–p π interaction by a factor of approximately $1/(4)^{1/2}$ (=0.5) because the normalization of the fragment orbital reduces the d$_{xy}$ contribution on a given metal atom by this factor. That is, the [fragment orbital]–O pπ overlap is correspondingly reduced. It is this smaller effective overlap which is responsible for the considerably reduced splitting in the delocalized Mo$_4$O$_2$ system.

In NaMo$_4$O$_6$ every crystal orbital is similarly delocalized over four metal atoms (although unequally), and hence the perturbation of the one-dimensional band structure will be similarly reduced as we introduce the Mo–O d–pπ interaction of the bridging oxides. In other words, the delocalization of a given crystal orbital over four metal atoms serves to reduce the contribution of the bridging oxide pπ orbitals in that particular crystal orbital. Note that we may *not* conclude the *overall* Mo d–pπ bonding is weaker because the total number of crystal orbitals is larger (the net contribution to Mo–O d–pπ bonding is spread over more bands). In any case, the discussion given here has been general and should apply as well to the systems discussed below. This offers some justification for our continued use of the one-dimensional model in the work that follows.

Distortions. New Compounds

Some newly synthesized quaternary molybdenum oxides reveal edge-sharing chains which have undergone a remarkable distortion. McCarley[26] and co-workers have found that in compounds with stoichiometries Sc$_{3/4}$Zn$_{5/4}$Mo$_4$O$_7$ and Ti$_{1/2}$Zn$_{3/2}$Mo$_4$O$_7$, molybdate chains similar to those in NaMo$_4$O$_6$ exhibit marked pairing between apical Mo atoms in the chains. In Figure 8 the Sc$_{3/4}$Zn$_{5/4}$Mo$_4$O$_7$ structure is shown. At top in this figure we have a view down the molybdate chain axes, revealing the essential similitude between these chains and those in NaMo$_4$O$_6$. The interchain linkage is, of course, different: the chains are bound together in layers through Mo–O bridges and these layers are in turn fused via Sc–O and Zn–O bonds. The details of Sc and Zn stoichiometry and site occupancy are discussed by McCarley. In the bottom view of Figure 8, we are looking down upon one of the "layers" described above. This view better reveals the Mo–Mo pairing within a chain; distances between basal Mo atoms remain regular while apical atoms are paired such that top and bottom apices show alternating long and short contacts which are opposite each other. This state of affairs is achieved by tilting adjacent Mo$_6$ octahedra rigidly, as illustrated for the molybdenum framework in **12**. In subsequent discussion we will describe this tilting by an angle φ which is the dihedral angle between the basal

(26) This material was presented as part of the ACS Symposium Series at Indiana University in May 1982. The conference was entitled "Inorganic Chemistry: Toward the 21st Century".
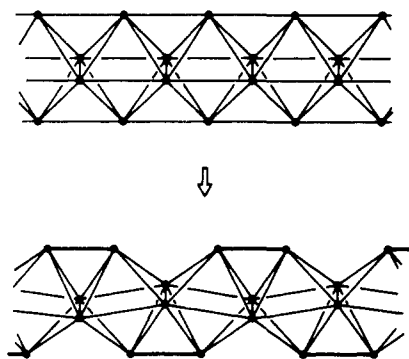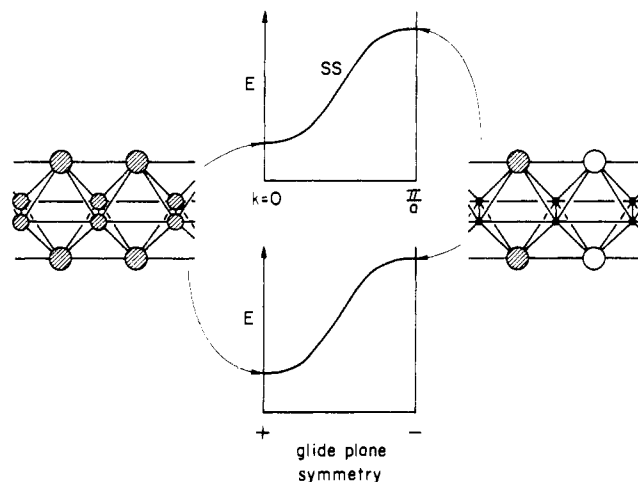
12

planes of adjacent octahedra and is 180° for the regular chain. The pairing between apical metals will be characterized by a distance Δ which is the difference between long and short Mo–Mo contacts between the apical atoms. For $Sc_{3/4}Zn_{5/4}Mo_4O_7$, $\varphi \simeq$ 173° and $\Delta = 0.51$ Å; in the isostructural $Ti_{1/2}Zn_{3/2}Mo_4O_7$, $\varphi \simeq 177°$ and $\Delta = 0.20$ Å.

Why should such distortions occur? Can our one-dimensional model shed light upon the origin of this intriguing structural anomaly? The theoretical results cited above are only of limited utility in answering these questions. We have found the overlap populations between apical molybdenums to be small and so this distortion could be rationalized on the grounds that the system might well sacrifice two weak Mo–Mo bonds to form one strong bond—as implied by **12**. The tilting distortion also does not stretch any bonds other than that between apical metals, an advantageous feature in light of our assessment of the greater strength of the other Mo–Mo bonds. At best, such an argument tells us that the motion described by **12** should be an easy one—we are left with little notion of why this distortion should be observed for any particular system.

It turns out that we can indeed derive insight into the reasons for the pairing distortion from our model, *if* we properly reexamine the basic symmetry properties of the system. In constructing the model band structure of Figure 4, we employed the vertical (xz) and horizontal (xy) mirror planes to classify the band symmetries. Implicit in that figure is, of course, the translational symmetry of the chain. Upon the onset of the distortion illustrated in **12**, we lose the horizontal mirror plane and the translational symmetry is altered so that there are twice as many atoms in the resulting translational unit cell. However, a glide plane operation (consisting of a reflection in the xy plane followed by a translation by half the length of the new primitive translation) is also present. In the undistorted system, this glide plane is a trivial consequence of the translational and xy mirror plane symmetry—for the distorted system it is preeminent. Indeed, to best study the undistorted structure as a prelude to distortion, one should abandon the translational symmetry in favor of the glide plane.[27]   (A parallel treatment would use the twofold screw axis that threads the chain; we have chosen the glide plane to satisfy our particular idiosyncrasies.)

The band structure of Figure 4 may be used to construct a new picture on the basis of the glide plane symmetry. To see this, we present some schematic examples—the orbitals we examine bear no resemblance to the crystal orbitals of the molybdate chains but are for illustrative purposes. Consider a hypothetical band as illustrated in **13**. This band bears an SS label according to its mirror plane symmetry and is plotted in two ways. At top is the usual plot, according to translational symmetry. At left is the orbital which is symmetric with respect to translation, and at right the antisymmetric orbital is found. In the bottom picture

---

(27) Note that the requirements of translational symmetry continue to be satisfied, *implicitly*. The glide plane operation plus the vertical mirror plane (and the horizontal mirror plane in the undistorted case) serve to generate all the symmetry operations of the chain. Our approach underlies the procedure of "unfolding" bands which is often seen in the literature.
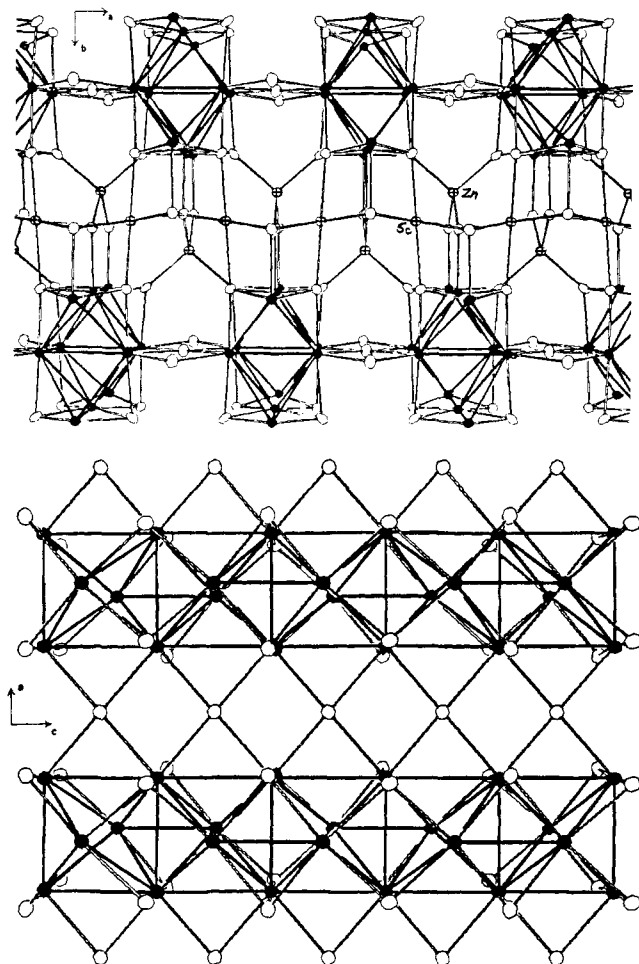
13

the same band is drawn so that at left is the orbital which is symmetric (+) with respect to reflection in the basal plane *plus* translation and at right is the antisymmetric (−) orbital. Now we consider another hypothetical case, the band displayed in **14**.
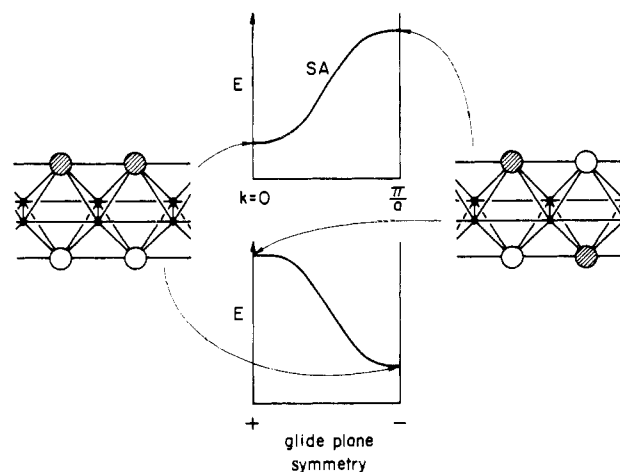
14

This band bears a SA label because the orbitals are symmetric with respect to reflection in the vertical plane and antisymmetric with respect to reflection in the basal plane. Note that the band in the lower picture is *reversed* with respect to the upper. Because the orbitals are antisymmetric with respect to reflection in the basal plane, those which were symmetric upon translation ($k = 0$) are antisymmetric upon the action of the glide plane (−) and vice versa.

The above examples point to a prescription: all bands which are antisymmetric with respect to reflection in the basal plane (i.e., bear an SA or AA label in Figure 4) should be *reversed*. Furthermore, since upon distortion the basal plane will be removed as a symmetry element (but *not* the glide plane), we should drop the second label altogether. Upon applying this prescription to our model band structure, we obtained that which is shown in Figure 9a. The S and A labels which remain are in reference to the crystal orbital symmetry with respect to reflection in the vertical mirror plane which is preserved during the tilting distortion. For convenience, we will continue to refer to these figures in terms of "zones" although we are not considering Brillouin zones in the conventional sense.

Because the bands in Figure 9a derive from a calculation on a system which was in fact *undistorted*, there remain crossings between bands which otherwise could not cross, that is, between bands of the same symmetry. These crossings are encircled in

Figure 8. The $Sc_{0.75}Zn_{1.25}Mo_4O_7$ structure, viewed down the chain axes and perpendicularly down upon a layer of linked chains. This view is a "top view" of the chains in the sense used heretofore in this paper.
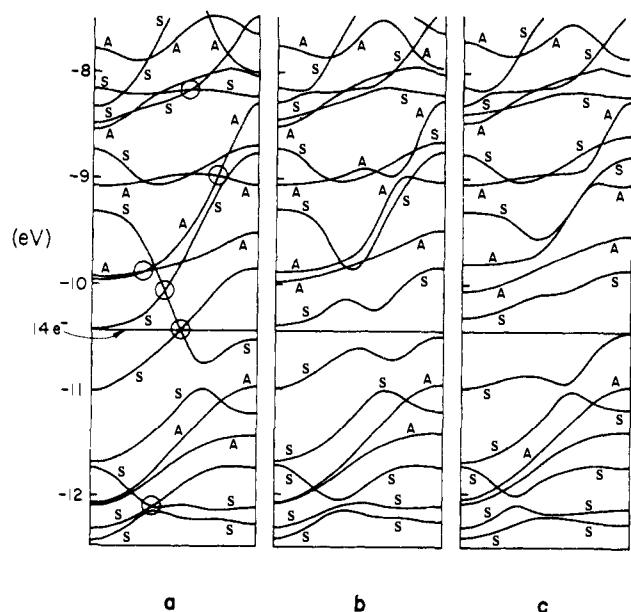

Figure 9. Energy bands for the tilted chains plotted by using glide plane symmetry. The bands in a are for the untilted chain. The circled crossings are discussed in the text. The bands for b and c correspond to tilted chains for which $\varphi = 178°$ ($\Delta = 0.13$ Å) and $\varphi = 174°$ ($\Delta = 0.41$ Å), respectively.

Figure 9a. The three highest energy crossings are of little interest because they involve high-lying bands which are unoccupied for systems with less than 20 electrons/Mo_4 unit. The lowest crossing
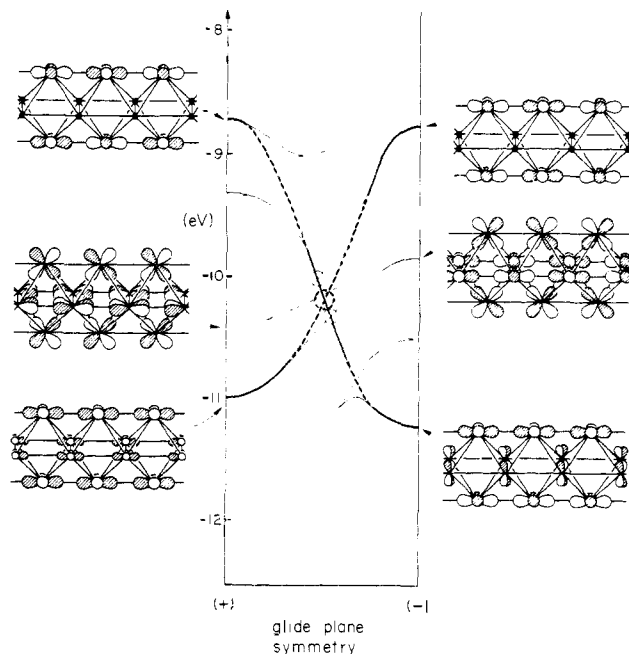

Figure 10. The essential bands for the tilting distortion. Dashed lines indicate the effect of ignoring interband mixing. $x^2 - y^2$ bands are indicated with heavy lines.

may be similarly ignored—the bands involved are occupied for systems of interest. The crossing between the two bands of A symmetry at just over −10 eV on our diagram is in a region of such low slope for both bands that its presence is of little consequence energetically; in any case, whether these bands actually *do* cross is questionable in light of the vagaries of our method of calculation. We are left with only two significant crossings: those involving bands of S symmetry between −10 and −11 eV in Figure 9a.

Should the Fermi level lie near one of these crossings, then we would expect the tilting distortion to be favored. The reason for this is that a distortion will open gaps at the crossings and thereby stabilize filled levels while destabilizing empty levels. Parts b and c of Figure 9 show the band structure which is obtained from calculations in which small ($\varphi = 178°$, $\Delta = 0.14$ Å) and large ($\varphi = 174°$, $\Delta = 0.41$ Å) excursions along the tilting distortion coordinate were made. The geometrical details are discussed in the Appendix. Before considering the effects of these distortions in detail, we will examine the orbitals involved in the band crossings—for now it is sufficient to note that distortion does indeed open gaps at the crossing points.

To uncover the essential driving force for the pairing of apical metals, we focus on the bands responsible for the crossings in which we are interested. In Figure 10 we show the bands of S symmetry which participate in this energy range. The dashed lines indicate the "natural" shape of the bands, that is, we decouple bands which are mixing in the interior of the zone. Inspection of the crystal orbitals in this figure make this decoupling natural; the orbital character at the zone boundaries are obviously similar for the three bands illustrated. When presented in this fashion, the two crossings discussed earlier coalesce into one effective crossing: that between the heavy lined bands in Figure 10. These are apical $x^2 - y^2$ bands which are either symmetric or antisymmetric with respect to the horizontal mirror plane lost in the tilting distortion. The simplicity of a single crossing is spoiled by the middle band illustrated in Figure 10. This band is built up from apical xz and basal atom contributions. As we shall see below, this band is effectively unperturbed by distortion. Thus, is is the apical $x^2 - y^2$ bands which are driving the tilting distortion.

The crossing of Figure 10 occurs near the midpoint between the zone boundaries. Hence, we will examine a schematic set of crystal orbitals appropriate to this point in the zone to discuss the "mechanism" of the tilting distortion. This discussion will neglect the interfering middle band of Figure 10. At top in Figure 11,
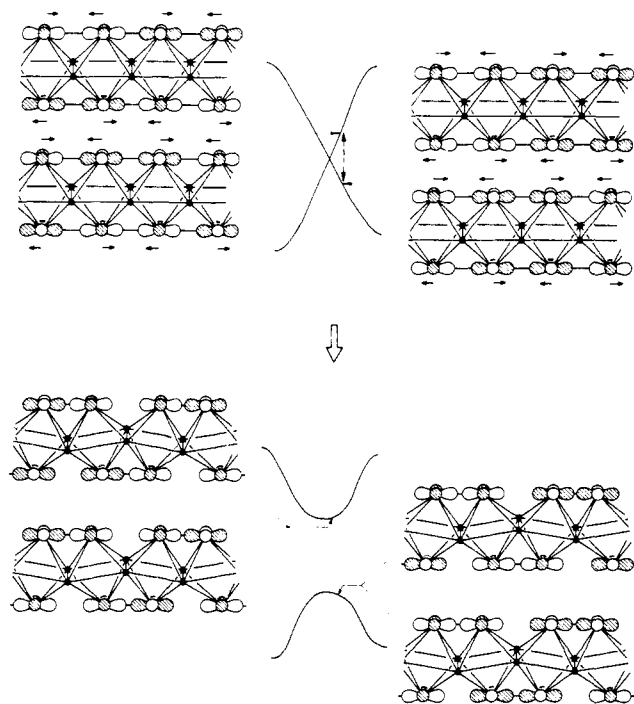
Figure 11. The effect of distortion upon the schematic apical $x^2 - y^2$ bands. The interband interaction turned on by tilting is indicated by the dashed line.

we show the $x^2 - y^2$ bands and crystal orbitals as they would appear at the zone midpoint, near the crossing emphasized in Figure 10. Each band is represented by a doubly degenerate set of crystal orbitals which are composed of linear combinations of a pair of complex conjugate orbitals belonging to "k" and "$-k$". Since we have two bands, four orbitals are shown; at left are crystal orbitals which are symmetric with respect to reflection in the horizontal mirror plane, at right—antisymmetric. The arrows in this figure represent the motion of the apical atoms during the tilting distortion.

The most notable feature of this distortion is that none of the crystal orbitals shown at top in Figure 11 are affected in "first order". That is, without mixing in orbitals from other bands, the degeneracies will not be lifted: for all the orbitals shown, the distortion turns on as many antibonding interactions as bonding. This situation contrasts with the usual "Peierls distortion" argument where splittings are indeed "first order". For example, in an NbX_4 chain we may consider the pairing observed between Nb atoms as having arisen from the splitting of a single $x^2 - y^2$ band[18,28] as in **15**. Mixing between bands is not necessary to
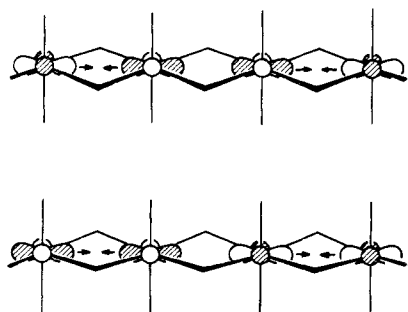
15

induce splittings in that case. In the molybdate case it is the

interaction introduced between the symmetric and antisymmetric $x^2 - y^2$ bands which is responsible for the pairing between apical Mo atoms. Because these two bands are so similar and the crossing between them is near the zone midpoint, the net effect is nevertheless quite similar to the usual Peierls distortion situation, as can be gleaned from the resultant crystal orbitals at the bottom of Figure 11. The formal situation distinguishing the present case from the more usual brand of Peierls distortion is comparable to the distinction between first-[29,30a] and second-order[29,30b,c] Jahn–Teller distortions.

What further inferences may we draw from our results? Returning to Figure 9, we see that the lowest six bands are largely unaffected throughout the distortion; however, we can see that a seventh and eighth band become distinct as the distortion proceeds. Particularly striking is stabilization of the seventh band upon distortion, most of which is seen in the interior of the zone. The eighth band is not stabilized upon distortion but rather it simply "flattens out" and loses the "wrinkle" it possessed in undistorted and weakly distorted cases. This eighth band is merely the middle band of Figure 10, reemergent. When the tilting distortion is large, the splitting of the apical $x^2 - y^2$ bands opens an effective gap so large that this band is no longer perturbed by the apical $x^2 - y^2$ bands. This is in accord with our ignoring this band as far as the pairing distortion is concerned, its function is to make the analysis more complicated! The stabilization of the seventh band results from the gap opened when the apical $x^2 - y^2$ bands interact. This results in a gap at the 14-electron level as a result of tilting, indicated in Figure 9.

Deciding what electron count should favor the largest tilting distortion on the basis of the band structure for the *undistorted* case is made problematic by the presence of the bothersome "middle band" of Figure 10. If the rule of thumb is to choose an electron count such that the Fermi level intersects a crossing, which crossing do we select? Do we focus upon the actual crossings of Figure 9a or the intended crossing of Figure 10? The former choice yields no definitive count because there are two crossings; the latter yields a count of ~ 14.8 e/Mo_4. In any case the question is probably academic since our method of calculation does not yield relative band energies so accurate as to enable such hair splitting. The accuracy of the one-dimensional model is also called into question at this point. The best that can be said is that systems with 13 or fewer electrons/Mo_4 need not distort and systems with 14–15 e should distort. We are thus unable to distinguish theoretically between $Sc_{0.75}Zn_{1.25}Mo_4O_7$ and $Ti_{0.5}$-$Zn_{1.5}Mo_4O_7$ which have formal electron counts of 14.75 and 14.5 e/Mo_4, respectively (the oxidation states assumed are Sc(III), Zn(II) and Ti(III)).[31]

The energetics of the tilting distortion as a function of electron count are conveyed in Figure 12 where relative total energy curves for 0-, 12-, and 14-electron occupancies are plotted as a function of the tile angle φ. The absolute changes upon distortion are less reliable in our calculations than the trend provided in comparing different occupancies. While the first 12 e are seen to only weakly affect the d^0 curve, occupation of the seventh band is driving the distortion. For the sake of computational economy, we did not optimize the structure as a function of tilting, although we did carry out enough calculations to determine that the EH method overestimates the tendency to distort. While this is largely a manifestation of this method's tendency to underestimate bond lengths (referring to the nascent bonds between apical metals), our one-dimensional model may neglect "strain" induced in the three-dimensional oxygen skeleton by the tilting distortion.

In our treatment of distorted systems we have entirely restricted ourselves to one-dimensional models. This approach, necessitated by computational limitations, ignores interchain interactions and

(28) Whangbo, M.-H.; Foshee, M. J. *Inorg. Chem.* **1981**, *20*, 113–118.

(29) Pearson, R. G. "Symmetry Rules for Chemical Reactions"; Wiley: New York, 1976.
(30) (a) Jahn, H. A.; Teller, E. *Proc. R. Soc. London, Ser. A* **1937**, *161*, 220–237. (b) Öpik, U.; Pryce, M. H. L. *Proc. R. Soc. London, Ser. A* **1957**, *238*, 425–447. (c) Bader, R. F. W. *Can. J. Chem.* **1962**, *40*, 1164–1175.
(31) The assignment of oxidation states is based on core level shifts in UPS data—McCarley, R., private communication.
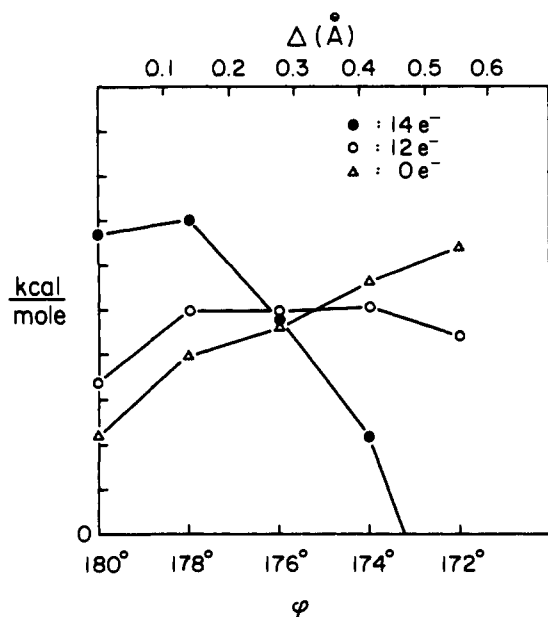
Figure 12. Relative energy curves for the tilting distortion with different band occupancies. The curves are arbitrarily shifted for presentation on one graph. The scale indicated by the vertical hash marks are kilocalories per mole of Mo_4.

Table III. Extended Hückel Parameters

orbital		H_{ii}, eV	$\zeta_1{}^b$	$\zeta_2{}^b$	$C_1{}^a$	$C_2{}^a$
Mo	4d	−11.06	4.54	1.90	0.5899	0.5899
	5s	−8.77	1.96			
	5p	−5.60	1.90			
O	2s	−32.3	2.275			
	2p	−14.8	2.275			

^{a} Coefficients used in double-ζ expansion. ^{b} Slater-type orbital exponents.

assumes counterions to be "innocent" donors. Probably the most serious structural approximation is the neglect of direct Mo–Mo contacts of ~3.2 Å in $Sc_{0.75}Zn_{1.25}Mo_4O_7$ and $Ti_{0.5}Zn_{1.5}Mo_4O_7$ between basal Mo atoms of adjacent chains (see Figure 8). This neglect will not seriously affect the conclusions concerning the tilting distortion since the orbitals involved are primarily localized on the apical molybdenums. However, other bands will be perturbed to a greater extent—including the middle band of Figure 10 which is largely localized on basal metal atoms. This naturally contributes to uncertainty regarding exactly what electron count will contribute to the largest distortions. Also dubious is the small gap that we find at the 14-electron level in distorted systems. This gap will likely be closed by interchain interactions.

Despite our model's limitations, it is clear that we have a good working understanding of the metal–metal bonding in this growing class of molybdate compounds. The model achieves more than merely satisfying our curiosity about Mo–Mo bonding in the beautiful $NaMo_4O_6$ structure; the reasons behind the distortions

observed in the new quaternary compounds are cleanly elucidated. The synthetic and physical chemistry of these systems continues to gather momentum. Hints of fresh surprises are emerging from systems in which different counterions are being intercalated. One obvious goal in this work would be the preparation of compounds with the $NaMo_4O_6$ type which are more electron rich (>14 e/Mo_4); these too should distort. A particularly fascinating prospect is the preparation of a system such as $PtMo_4O_6 = Pt^{2+}(Mo_4O_6{}^{2-})$ in which d^8 platinum would occupy *square-planar* sites in the channels between molybdate chains. Some distortion of the $NaMo_4O_6$ structure would probably be required in order to provide a sufficiently small "hole" for Pt as a Pt–O distance of 2.34 Å would otherwise result. The preparation of such a system leaves open the question of whether charge transfer from the platinums might formally exceed two electrons in order to empty the top of the Pt "z^2 band". The possibilities for metal–metal bonding *within* the channels of these systems is intriguing, and we eagerly await the further unfolding of the chemistry of these compounds.

Appendix

The extended Hückel method was used in all calculations; parameters for molybdenum[32] and oxygen appear in Table III. Mo–O bond lengths involving trigonal oxygens were taken as 2.01 Å, all other Mo–O distances were set at 2.07 Å. All Mo–O distances were maintained in calculations on distorted chains. Except for distances between apical Mo's, all Mo–Mo contacts were taken to be 2.8 Å throughout. Energy band curves and total energies were calculated by using the smooth Fourier interpolation method of Kertesz and Hughbanks.[33] DOS curves and weighted DOS curves displayed in Figures 4 and 7 were obtained from calculations including 41 k points of the one-dimensional irreducible Brillouin zone and smoothed with Gaussian functions with a half-width of 0.1 eV. In lattice sums, matrix elements between atoms separated by greater than 7.1 Å were taken as zero—using the criteria specified by Kertesz[34] et al.

(32) Kubacek, P.; Hoffmann, R.; Havlas, Z. *Organometallics* **1982**, *1*, 180–188.
(33) Kertész, M.; Hughbanks, T. *Phys. Rev. B* **1981**, *24*, 6870–6879.
(34) Kertész, M.; Koller, J.; Azman, A. *Lect. Notes Phys.* **1980**, *113*, 56–79.